## ARTICLES

# Interplay between electron-electron interaction and electron-phonon coupling near the Fermi surface of $1T$-$TaS_2$

Th. Pillo,[1,*] J. Hayoz,[1] H. Berger,[2] R. Fasel,[1] L. Schlapbach,[1] and P. Aebi[1]
[1]*Institut de Physique, Université de Fribourg, CH-1700 Fribourg, Switzerland*
[2]*Institut de Physique Appliquée, EPF, CH-1015 Lausanne, Switzerland*
(Received 18 October 1999; revised manuscript received 29 February 2000)

We present a detailed high-resolution angle-resolved photoemission study of the electronic band structure of the room-temperature quasicommensurate charge-density-wave phase of $1T$-$TaS_2$. In particular, we show that no crossings of the Fermi level are visible in the complete Brillouin zone, indicating that an electron-electron correlation-induced pseudogap in the Ta $5d$ derived band exists already above the Mott localization-induced transition at 180 K. Moreover, we find that the electronic structure is governed by at least two quasiparticle peaks, which can be assigned to electrons from starlike shells of Ta atoms within the distorted crystal lattice. These peaks show quasilocalized (dispersionless) behavior in parts of the Brillouin zone where the one-particle band is unoccupied and they follow the one-particle dispersion in the occupied part. In order to address the question of possible Fermi-surface (FS) nesting, we scanned the remaining remnant FS and found regions with a considerable decrease of spectral weight. However, we find no clear evidence for FS nesting.

### I. INTRODUCTION

Layered transition metal chalcogenides (TMC's) have stimulated ongoing experimental work since more than three decades because of their quasi-two-dimensionality (2D) and, consequently, their unique physical properties.[1,2] In particular, improved experimental equipment and insights gained from studies of the high-temperature superconducting cuprates (HTSC) renewed interest and attention for $1T$- and $2H$-type TMC's. Especially, surface-sensitive techniques such as angle-resolved photoemission spectroscopy[3] (ARPES) and scanning tunneling microscopy[4] (STM) led to insights in the mechanisms behind the puzzling behavior of these TMC's.

Among them, $1T$-$TaS_2$ plays a major role because its phase diagram exhibits a variety of phase transitions.[1,5] The formation of a $\sqrt{13}\times\sqrt{13}$ superstructure passes several precursor states from the incommensurate ($I$) via the quasicommensurate (QC) to the final low-temperature commensurate ($C$) phase below 180 K.[2] Obviously, the electronic structure, especially in the vicinity of the Fermi level $E_F$, displays characteristic features correlated to this superstructure. In particular, a Mott-Hubbard transition occurring at 180 K revealed the importance of electron correlation effects in the Ta $5d$ band.[6] On the one hand these Coulombic effects lead to a (Mott) localization of electrons, on the other hand the Fermi-surface (FS) topology, as deduced from band-structure calculations, seems to yield suitable conditions for FS nesting.[7,8] Whereas the QC-$C$ phase transition and the $C$ phase have been examined by ARPES (Refs. 9–17) and STM (Refs. 18–22) work, the influence of the CDW superstructure at room temperature (RT) in the QC phase on the *overall* band structure, especially away from high-symmetry directions, has experimentally not been considered in great detail.

Consequently, the aim of this study shall be to investigate the electronic band structure near and at $E_F$ throughout the Brillouin zone (BZ) by means of scanned ARPES (ScARPES) in the QC phase. We especially addressed the question of possible FS nesting fingerprints and/or localization in the intermediate QC phase. Surprisingly, we find no evidence of a Fermi-level crossing of the Ta $5d$ band,[23] instead we find a back dispersion of the Ta $5d$ band at the normal state Fermi vector $\mathbf{k}_F$ due to the opening of a correlation pseudogap and leaving a remnant Fermi surface (RFS) already at RT. The interpretation of the opening of a correlation gap throughout the BZ is corroborated by a comparison to RT-ARPES experiments of the parent TMC $2H$-$TaSe_2$, a metallic system, where the Ta $5d$ band crosses the Fermi level and is not perturbed.

Furthermore, the overall band structure away from high-symmetry directions is dominated by at least two quasiparticle (QP) peaks sitting on an incoherent background. They exhibit a small bandwidth and practically no dispersion in the region where the one-particle $5d$ band, as predicted by band-structure calculations,[7,8] is unoccupied. In the occupied parts, however, their dispersion follows what is expected from the one-particle band.

Scanning the FS contour of $1T$-$TaS_2$ reveals regions with reduced spectral weight but we only find evidence for, if at all, imperfectly nested areas of the (remnant) FS. Comparing these regions with our azimuthal dispersion plots, however, leads us to the conclusion that they represent effects of the band structure instead of being experimental evidence for gaps.

This paper is organized as follows. In Sec. II a summary of relevant properties of $1T$-$TaS_2$ is given. Section III de-

 

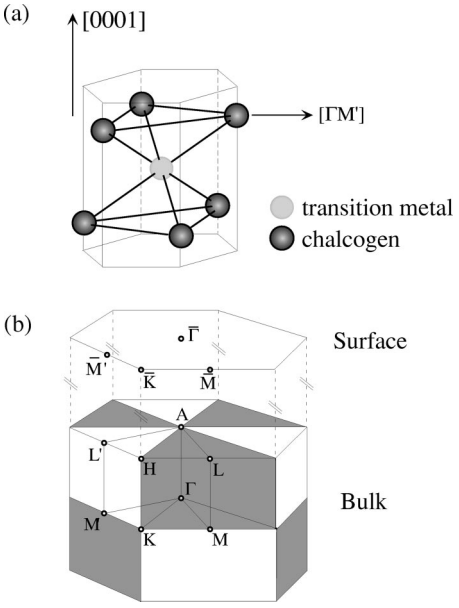


FIG. 1. (a) Sketch of the $CdI_2$-type structure present in $1T$-$TaS_2$. High-symmetry directions are indexed by the arrows. Dark gray spheres denote the chalcogen atoms. (b) Drawing of the Brillouin zone of the $CdI_2$-type structure. High-symmetry points are labeled. Note the necessity to distinguish between $M(L)$ and $M'(L')$ points due to the trigonal symmetry (see text). The corresponding surface Brillouin zone is indicated.

scribes the experimental setup and the calculations. In Sec. IV we show our results and try to give a consistent picture of the **k**-resolved band structure of $1T$-$TaS_2$. We finish with a summary in Sec. V.

## II. STRUCTURAL PROPERTIES, CDW's, AND LOCALIZATION

$1T$-$TaS_2$ crystallizes in the $CdI_2$-type structure with the space group $D_{3d}^3$.[1] Ta atoms form a hexagonal sheet and are sandwiched between sheets of hexagonally arranged S atoms as shown in Fig. 1(a). The plane parallel to the sheets [the (001) or (0001) plane] is exposed when cleaving the samples because of weak van der Waals interlayer coupling between neighboring sandwiches. In the $1T$ phase, the Ta atoms are octahedrally coordinated by the S atoms in contrast to the $2H$ type where an adjacent rotated unit cell is added in the perpendicular direction making the coordination trigonally prismatic. The intracell symmetry in the $1T$ polytype is, hence, trigonal calling for a distinction between the $[\overline{\Gamma M}]$ and the $[\overline{\Gamma M'}]$ direction in reciprocal space, as indicated in Fig. 1(b) where the bulk as well as the surface Brillouin zones (SBZ) are shown. In the sketch, high-symmetry directions and points are given together with the irreducible zone (delimited by thin gray lines) due to the trigonal symmetry. As a consequence, the band-structure reflects the trigonal symmetry and, hence, the borderlines between the shaded and unshaded areas are symmetry equivalent whereas the interior of the areas is not.[24] The determination of the $[\overline{\Gamma M'}]$ azimuth is straightforward considering the real-space geometry. It is given by the direction towards the topmost S atoms. The different crystal geometries of the hexagonal $2H$ and the trigonal $1T$ polytypes can be seen very easily in x-ray photoelectron diffraction (XPD) patterns.[24,25] This facilitates the (experimental) determination of the $[\overline{\Gamma M}]$ and the $[\overline{\Gamma M'}]$ directions.

The electronic structure of $1T$-$TaS_2$ can, in a purely ionic picture, be described by the bonding and antibonding bands of the S $3p$ and Ta $6s/6p$ orbitals.[1] Conduction is given by the Ta $5d$ derived conduction band situated in a large bonding-antibonding band gap of 8 eV. Considering the octahedral coordination the Ta $5d$ band is split off into $t_{2g}$ and $e_g$ manifolds. The slight perpendicular distortion removes the degeneracy and one is left with three subbands from the $t_{2g}$ manifold and the two bands from the $e_g$ manifold. The metallic character of $1T$-$TaS_2$, nevertheless, comes from the $d_{z^2}$ band which is partly filled. The other manifolds are unoccupied.

$1T$ dichalcogenides are known to be the first 2D materials where charge density waves (CDW) have been seen experimentally by means of superlattice spots in x-ray diffraction.[26] In contrast to $2H$ polytypes, the $1T$-type materials show a very large CDW amplitude as revealed by STM.[4] As a consequence of the CDW's $1T$-$TaS_2$ exhibits a very rich phase diagram as a function of temperature.[2] The undistorted phase exists only in a very narrow temperature range above 550 K. At about 570 K an irreversible transition to the trigonal prismatic phase occurs. Upon cooling, $1T$-$TaS_2$ shows an incommensurate (IC) CDW from 550 K down to 350 K, where the CDW becomes quasicommensurate (QC). Further cooling reveals another first-order phase transition at 180 K, where the CDW becomes commensurate ($C$) with the underlying lattice. Reannealing yields a large hysteresis in the QC-$C$ transition.[27,28] The $C$ phase is manifest by a $\sqrt{13}\times\sqrt{13}$ superlattice, which is built of 13 Ta atoms forming a so-called ''Star-of-David'' cluster.[2,6] A possible expansion of the CDW's also in the direction perpendicular to the layers has been discussed[29,30] but no clear proof has been given. For other $1T$ compounds, this may be important as shown for $1T$-$TiSe_2$, where $k_\perp$ effects have been found to be non-negligible and the material also reconstructs along the $c$ direction having considerable influence on the band structure.[31]

Figure 2(a) shows the $\sqrt{13}\times\sqrt{13}$ superlattice (in the Ta plane) as the dashed rhombic structure. The periodic lattice distortion (PLD) coupled to the CDW formation (shown as small arrows) displaces the Ta atoms (hollow circles) such that out of 13 Ta atoms six atoms each form two outer shells with one Ta atom left in the center of the star.[6] Figure 2(b) shows a low-energy electron-diffraction (LEED) experiment of the QC phase with high intensity given as black. The large hexagons represent the SBZ and the small hexagons the one due to the $\sqrt{13}\times\sqrt{13}$ superlattice. LEED data for the $C$ phase (not shown) reveal the same surface structure, but with more intense satellite diffraction peaks and a slightly larger rotation angle being completely consistent with the ''Star-of-David'' model of Fazekas and Tosatti (FT). Finally, Fig. 2(c) depicts a typical curve for the in-plane resistivity $\rho$ as a function of temperature (taken from Ref. 27). On top of the plot, the temperature extension of the different CDW phases occuring in $1T$-$TaS_2$ as mentioned is sketched for the sake of convenience.

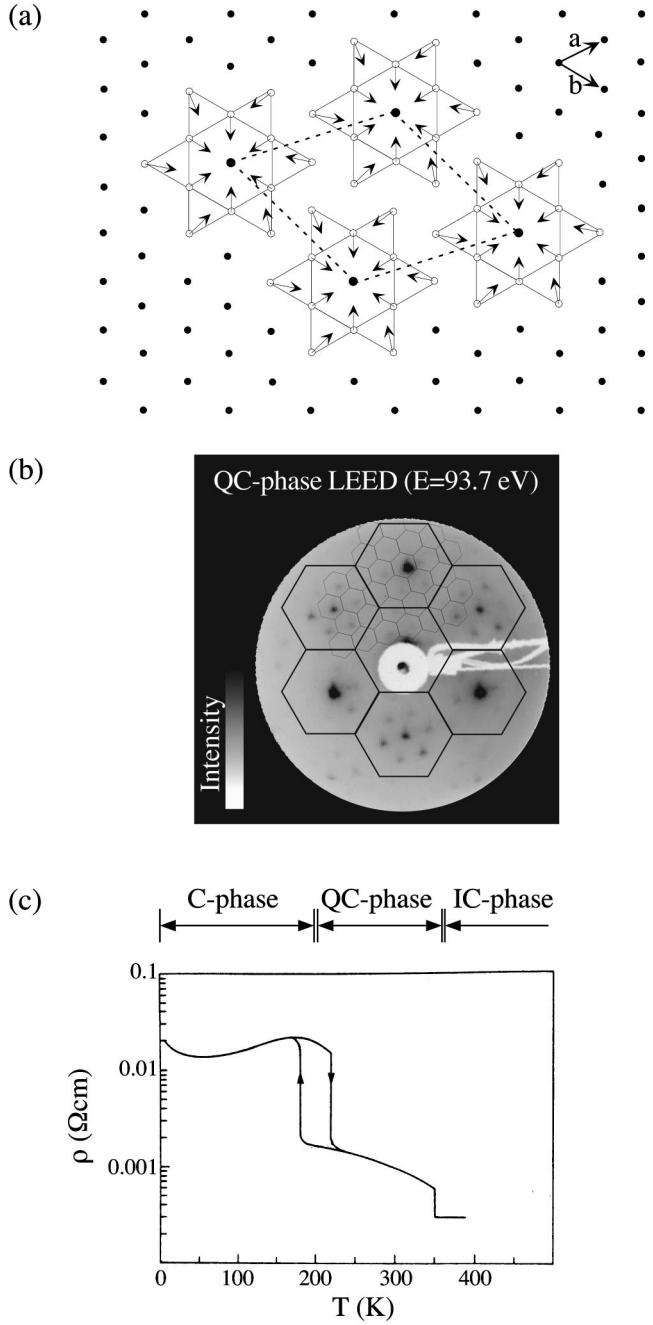


FIG. 2. (a) Ta basal plane yielding the $(1\times1)$ symmetry and the ''Star-of-David'' clusters caused by the $(\sqrt{13}\times\sqrt{13})$ superstucture in the commensurate CDW phase. The arrows give the lattice distortions on the Ta sites. The new unit cell in real space is given by the dashed rhombus. (b) Low-energy electron diffraction (LEED) experiment (kinetic energy 93.7 eV) of the QC phase. The unreconstructed SBZ and the superstructure SBZ are indicated by the large (small) hexagons, respectively. (c) Typical in-plane ($\perp$ to the layers) resistivity curve as a function of temperature of $1T$-$TaS_2$ (taken from Ref. 27). The CDW phases occurring are added on top of the resistivity plot.

The microscopic structure of the QC phase has been a matter of debate for almost a decade untill the pioneering work of Wu *et al.*[18] who showed by STM that the QC phase consists of hexagonally arranged commensurate domains being separated by soliton walls. Upon cooling to cryogenic temperatures the commensurate domains seem to grow untill the complete lock-in, i.e., the sudden disappearance of the solitons at 180 K. The influence of the CDW potential on the $d_{z^2}$ derived band is expressed by a decay of its density of states (DOS) into three satellite structures.[12] There are two small satellites and a prominent peak, e.g., displayed in ARPES spectra.[9,12–16] According to the model of FT [Fig. 2(a)] each of the two small satellites is attributed to electrons within one of the two centered shells consisting of six Ta atoms. The third prominent peak represents the remaining thirteenth electron in the center of the cluster which becomes susceptible to a localization-induced Mott transition at 180 K.[6] The long-range ordering of localized moments (i.e., the electron from the central Ta atom) does not lead to antiferromagnetism because the lattice is trigonal and it is not possible to arrange $\uparrow\downarrow$ pairs antiferromagnetically on such a lattice. Another argument was put forward by Geertsma *et al.*,[32] who showed that the ground state of a single *d* electron in a cubic environment exhibits a first-order Zeeman splitting equal to zero. However, as argued by FT,[6] the outcome, if including all crystal-field effects, would be an anisotropic susceptibility being much smaller than the one for 13 free spins on the star centers.

Due to electron-electron interaction the $d_{z^2}$ band is split off upon cooling into an upper unoccupied Hubbard band (UHB) and a corresponding lower Hubbard band (LHB). The LHB is manifest as a dispersionless peak near $E_F$ in near-normal emission ARPES spectra of the *C* phase.[12–17] The splitting is symmetric with respect to $E_F$ as evidenced by tunneling spectroscopy data[22] and shows a correlation gap of about 180 meV.[12–17] Temperature-dependent ARPES work showed that the correlation gap in the DOS is actually a pseudogap below 180 K with residual spectral weight at $E_F$ down to low temperatures.[15,16] Furthermore, $1T$-$TaS_2$ shows a pseudogapped Fermi surface already at room temperature, possibly as a precursor of the underlying Mott transition[23] whereby the effective local Coulomb correlation energy depends on random disorder.[17]

Independent of electron localization at low temperature, the CDW has to be driven by another mechanism. In one dimension (1D), electron-phonon coupling leads to the formation of electron-hole pairs on and near the FS with a subsequent removal of the FS and the opening of the so-called Peierls gap.[33,34] The concurrent PLD drives a softening of the corresponding phonon mode at $\vec{q}=2\mathbf{k}_F$ and finally the system lowers its free energy. This Peierls transition in 1D (Ref. 34) can be achieved only approximatively in 2D, either by large parallel areas of the FS (i.e., a large number of possible electron-hole pairs) or by a strong electron-phonon coupling parameter $\lambda$.[33] In that context, FS nesting seems to be the appropriate candidate, because band-structure calculations revealed a Fermi surface built up by elliptic electron pockets from the Ta $5d$ band around the *M* point of the BZ.[7,8] Experimentally, only the very existence of a CDW vector corresponding to the $\sqrt{13}\times\sqrt{13}$ superlattice is given.[26,35] In fact, a Peierls gap should be visible already at RT, but there is, to our knowledge, no experimental proof.

Here we shall present a detailed study of the band structure using a combination of scanning the FS contour via ARPES and mapping of almost the complete **k** space with

particular emphasis on regions away from the high-symmetry directions.

## III. EXPERIMENTAL DETAILS AND CALCULATIONS

The photoemission experiments were performed in a VG ESCALAB Mk II spectrometer with a base pressure $\leqslant 2 \times 10^{-11}$ mbar. Our sample goniometer is constructed for motorized, computer-controlled data acquisition over a $2\pi$ solid angle[36] and can be cooled with $LN_2$ down to 140 K.[37] X-ray photoelectron spectroscopy was used to check the cleanness of the sample. Unless stated otherwise, the ARPES measurements were performed with monochromatized He I$\alpha$ (21.2 eV) and H Ly$\alpha$ radiation (10.2 eV). The setup including the plasma discharge lamp and the VUV toroidal grating monochromator is described elsewhere.[38] The energy resolution is 20 meV for the He I$\alpha$ measurements and less than 100 meV for the measurements with hydrogen as discharge gas.

Pure samples of $1T$-$TaS_2$ and $2H$-$TaSe_2$ were prepared with the chemical vapor transport method. The samples were cut with a blade to the desired shape and mounted with silver epoxy on a polycrystalline Cu sampleholder. All $1T$-$TaS_2$ samples showed clear first-order phase transitions at 180 K (Ref. 39) indicating very good crystal quality.

Samples were oriented *in situ* with x-ray photoelectron diffraction (XPD) which provides high-symmetry directions very precisely. Angles can be scanned continuously to perform mappings of intensity at a constant energy such as $E_F$. Briefly, in such a Fermi-surface mapping (FSM) experiment, the spectral function in a small, resolution-limited energy window centered at $E_F$ is scanned over a nearly $2\pi$ solid angle and represented in a gray scale plot as a function of the polar and the azimuthal angle. This technique is well established, and has proven its power in mapping the FS of cuprates[40] or transition metals[24,41–44] as well as surface alloys.[45] For a review see Ref. 43.

In order to clarify our experimental results we performed-band structure calculations of bulk $1T$-$TaS_2$ in the undistorted phase using the full potential linearized augmented plane-wave (FLAPW) method[46] in the framework of the generalized gradient approximation.[47] The lattice parameters of the $D_{3d}^3$ space group were chosen to be $a=3.36$ Å and $c=5.90$ Å, respectively. For comparison with the experiment, we assumed a free-electron final state using a work function of 4.6 eV and an inner potential of 10 eV.[48] Energy eigenvalues were calculated along the final-state momenta and a linear gray scale is used to indicate energy conservation with black corresponding to a perfect coincidence of initial and final states.

## IV. RESULTS AND DISCUSSION

### A. Band mapping

#### 1. Γ*ALM plane*

First, we shall address the question of the behavior of the crystal-field split Ta $5d$ derived band along the high-symmetry direction $[\overline{\Gamma M}]$. Photoemission data for $[\overline{\Gamma M}]$ tend to state a real Fermi-level crossing of the Ta $5d$ band.[12,13] Our recent finding of a pseudogapped remnant FS (RFS) in the QC phase[23] calls for further investigation and we will present it here. Figure 3(a) presents a bulk band-structure calculation for the undistorted phase as described above. A parallel momentum of $k_\parallel = 0$ Å$^{-1}$ denotes normal emission ($\overline{\Gamma}$) and $k_\parallel = 1.08$ Å$^{-1}$ corresponds to the $\overline{M}$ point in the surface BZ when assuming a work function of 4.6 eV. Additionally, this calculation has been multiplied with a Fermi-Dirac cut-off function with a temperature of $T=300$ K in order to facilitate comparison with Fig. 3(b), where the corresponding experiment is shown, performed at RT with He I$\alpha$ radiation (21.2 eV).[49]

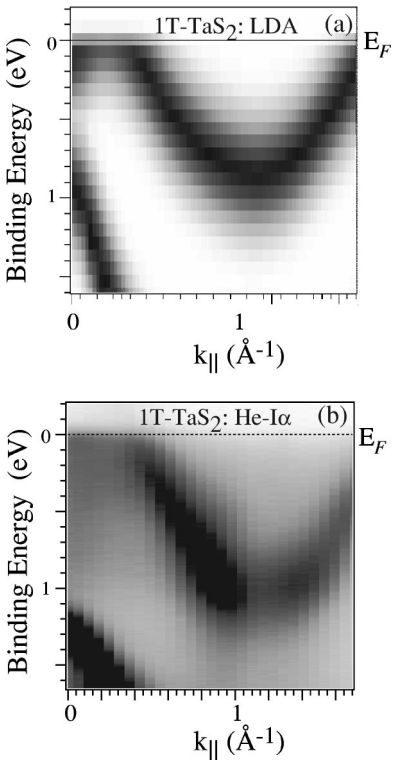


FIG. 3. (a) FLAPW calculation [within the local-density approximation (LDA)] for $1T$-$TaS_2$ in the ΓALM plane of the BZ for a photon energy of 21.2 eV, an inner potential of 10 eV, and a work function of 4.6 eV, respectively, in the approximation of free-electron final states. The plot has been multiplied with a Fermi-Dirac cut off function for 300 K. For details see text. (b) Corresponding measurement of $1T$-$TaS_2$. Linear gray scale ARPES dispersion plot using He I$\alpha$ radiation (21.2 eV). In both panels, $\mathbf{k}_\parallel$ counts along $[\overline{\Gamma M}]$ of the SBZ, or, in other words, in the Γ*ALM* plane.

The calculation [3(a)] clearly shows the undistorted one-particle Ta $5d$ derived band *crossing* the Fermi level at about 0.4 Å$^{-1}$ ($\mathbf{k}_{F1}$). A second branch of the Ta band crosses $E_F$ at a smaller momentum of approximately 0.1 Å$^{-1}$. This second band has been a matter of controversy in the literature.[7,8,50] In addition, the S $3p$ derived band shows up at about 1 eV binding energy at $\overline{\Gamma}$. We will not go into further detail concerning the calculation because our goal is not to optimize band-structure calculations of the undistorted phase but rather to understand the peculiar spectroscopic features of the QC phase. Comparing the experiment to the calculation, one can see the *S* band at a binding energy of about 1.4

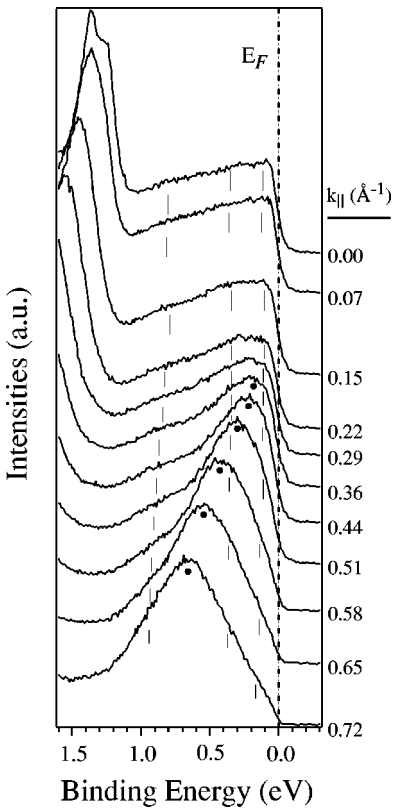


FIG. 4. Selected ARPES spectra for $1T$-$TaS_2$ along $[\overline{\Gamma M}]$ from the dispersion plot in Fig. 3(b). The black circles denote the positions of the quasiparticle Ta $5d$ band whereas the ticks indicate the CDW-induced satellites. The dashed line denotes the Fermi energy. Shown are spectra from normal emission ($k_\parallel = 0.0$ Å$^{-1}$) to a parallel momentum of $k_\parallel = 0.72$ Å$^{-1}$, approximately 3/4 of the $\Gamma$-$M(L)$ distance.

eV at $\overline{\Gamma}$. The Ta $5d$ derived band can be seen with a nearly parabolic shape with the apex at the $\overline{M}$ point. It coincides well with theory but there are several points to emphasize. First, the intensity of the quasiparticle (QP) peak is suppressed considerably on approaching $E_F$ and the QP does not really seem to cross $E_F$. Second, between $\overline{\Gamma}$ and $k_\parallel = 0.4$ Å$^{-1}$ a faint gray, incoherent background is visible. Finally, matrix elements (intensities) seem to differ distinctly between the first BZ (i.e., along the $[\overline{\Gamma M}]$ azimuth and the second BZ, where one is along the $[\overline{\Gamma M'}]$ azimuth. This observation has been reported previously for ARPES and inverse photoemission data.[13,48] Moreover, we stress that we do not detect spectral features related to backfolded BZ's caused by the $\sqrt{13}\times\sqrt{13}$ superstructure.

It is not clear now whether the dispersing state (denoted as the QP band throughout) visible in the ARPES spectra crosses $E_F$ or not. In Fig. 4 ARPES spectra from the dispersion plot (Fig. 3) are presented ranging from normal emission up to a parallel momentum of $k_\parallel = 0.72$ Å$^{-1}$. There are two distinct spectral features visible related to Ta $5d$ states. First, the dispersing QP peak (black circles) and, second, an incoherent background, expressed by three faint bumps in the spectra between $k_\parallel = 0.0$ Å$^{-1}$ and $k_\parallel = 0.29$ Å$^{-1}$ and as shoulders in the strong QP peak (indicated by the ticks, respectively). The behavior of these features is distinctly different. The QP peak disperses towards $E_F$ but, as we will see, does not cross it, and the satellites are nearly dispersionless. Both features are nicely reproduced in calculations, i.e., the QP peak in conventional band-structure calculations[7,8] (including our own) and the satellite peaks in the tight-binding calculation of Smith *et al.*[12] The QP peak is the one-particle-like Ta $5d$ derived band whereas the satellites represent the weakly dispersing bands caused by the CDW potential. Strictly speaking, the high- (binding) energy satellites correspond to the two outer shells in the FT model whereas the satellite near $E_F$ represents the central $d$ electron evolving into the lower Hubbard band (LHB) upon decreasing the temperature. The latter becomes much stronger in the $C$ phase where it is then responsible for the correlation pseudogap of 180 meV.[15,16] More precisely, the QP peak approaches $E_F$ untill a minimum binding energy of about 150 meV and then seems to show a slight backdispersing. This is intriguing because for a true crossing of $E_F$, this peak should come closer to $E_F$, at least to the limit which is given by $4k_BT = 100$ meV (i.e., the width of the Fermi distribution) for 300 K ($k_B$ is Boltzmann's constant). Also, the QP peak does not lose all its spectral weight as would occur if it crossed $E_F$. More importantly, in all spectra the Fermi level stays in the low intensities tail *below* the midpoint of the leading edge. This would not be the case if the peak really crossed $E_F$. Then, the finite width of the Fermi function would cause the Fermi level to be situated *above* the midpoint of the leading edge as will be illustrated below for the case of $2H$-$TaSe_2$.

Furthermore, we do not find spectral evidence for a second Ta band crossing $E_F$ near $\overline{\Gamma}$. This coincides with other ARPES work.[13,17] Therefore, either the calculations are inaccurate or it displays the scenario where the Ta band shows a similar backfolding in the unoccupied energy range.

For the sake of comparison, we carried out ARPES measurements on $2H$-$TaSe_2$, a layered TMC as well, but a trigonal prismatic polytype which shows a double stacking of the Se-Ta-Se sandwiches along the $c$ axis.[1] $2H$-$TaSe_2$ shows two CDW transitions, one into an incommensurate phase at 122 K, and a second one into a commensurate CDW phase at 90 K,[2] yielding a $(\sqrt{3}\times\sqrt{3})$ superstructure, oriented along the same axes as the unreconstructed lattice, in contrast to $1T$-$TaS_2$, where we have a rotation angle of $\approx 13°$. Several ARPES studies have been performed on $2H$-$TaSe_2$,[12,51,52] all indicating that in the $\Gamma ALM$ plane the Ta $5d$ derived band crosses $E_F$ and disperses parabolically towards the $\overline{M}$ point as apex. Therefore, this band is the direct analog to the Ta $5d$ band in $1T$-$TaS_2$. We measured ARPES spectra in the $\Gamma ALM$-plane with He I$\alpha$ radiation at RT. The results are presented in Fig. 5(a). On comparing this dispersion plot with that of $1T$-$TaS_2$ [see Fig. 3(b)], one observes that the spectral weight shows the abrupt decrease only at the energy position where the Fermi-Dirac distribution has to be taken into account, i.e., less than $\approx 100$ meV below $E_F$, and not before. The corresponding spectra are shown in Fig. 5(b), where we displayed only spectra up to the $\overline{M}$ point. Two selected spectra are marked by arrows. These spectra indicate the approximate location of the Fermi vector $\mathbf{k}_F(2H\text{-}TaSe_2)$. Here, one can see a clear $E_F$ crossing of the

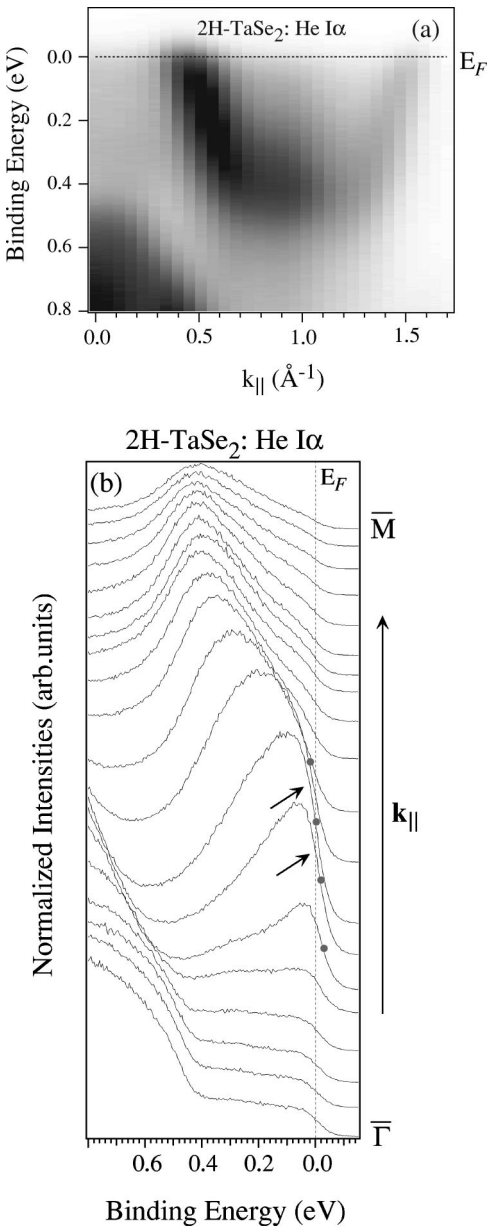


FIG. 5. (a) Dispersion plot in the $\Gamma ALM$ plane for $2H$-$TaSe_2$. Spectra have been collected with monochromatized He I$\alpha$ radiation. (b) Selected ARPES spectra from the $M(L)$ point down to normal emission ($\Gamma$). The two arrows indicate the **k** vectors between which the Ta $5d$ band *crosses* the Fermi level. For details see text.

Ta $5d$ band, which is rather broad due to the fact that one has actually two bands because of two formula units per unit cell in the $2H$ polytypes. Two arguments for this $E_F$ crossing can be put forward. First, the spectral weight decreases not before the peak has reached a binding energy of less than 100 meV. Second, perhaps the clearest indication, the Fermi energy, which refers to a binding energy of 0.0 eV, appears to be shifted within the leading edge. The respective midpoints of the leading edge are indicated by the small circles drawn on the spectra. The intensity at the midpoint of the leading edge is much smaller than the one at the experimental Fermi energy, which has been carefully determined by measuring the Fermi edge of the polycrystalline Cu sample holder on which the TMC samples are mounted. This is proof that

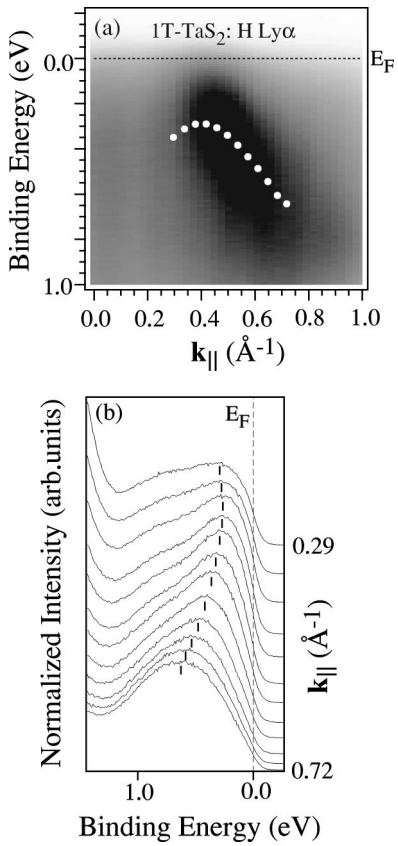


FIG. 6. Similar measurement of $1T$-$TaS_2$ to that of Fig. 3 but now with H Ly$\alpha$ radiation. (a) ARPES dispersion plot of the $\Gamma ALM$ plane with 10.2 eV. High intensity corresponds to black. The white circles denote peak positions taken from the spectra [cf. (b)]. (b) Selected ARPES spectra from the dispersion plot in (a) for parallel momenta from 0.29 to 0.72 $\text{Å}^{-1}$. The ticks on the peaks correspond to the circles in (a).

spectral weight has dispersed through $E_F$ and has its maximum in the unoccupied range.[24,53]

To exclude effects due to the 3D nature of the band structure of $1T$-$TaS_2$, we measured a dispersion plot in the same plane as before, but now with H Ly$\alpha$ radiation (10.2 eV) probing **k** points with different perpendicular momenta. The results are shown in Fig. 6. Figure 6(a) gives a linear gray scale plot with the maximum intensity as black. Note that because of the lower photon energy, we do not reach as far out in the momentum plane as before with He I$\alpha$. However, we have more points per $k_\parallel$ unit, in other words a better $k_\parallel$ resolution as compared to measurements with He I$\alpha$. White circles indicate the peak positions taken from selected ARPES spectra shown in Fig. 6(b). Here, peak positions are indicated by ticks. The QP band approaches $E_F$, but it does not cross the chemical potential. This is corroborated again by the position of the Fermi level within the leading edge which stays below the midpoint. All in all, the dispersion behavior of the ARPES spectra with 21.2 and 10.2 eV appears identical. The one-particle-like QP peak does *not* cross $E_F$, rather it exhibits a backdispersing at the Fermi vector $\mathbf{k}_F$ of the unperturbed Ta $5d$ band. Therefore, we can unequivocally conclude that for $1T$-$TaS_2$ we observe *no* $E_F$ crossing in the $\Gamma ALM$ plane, whereas in the case of $2H$-$TaSe_2$, there is an $E_F$ crossing.

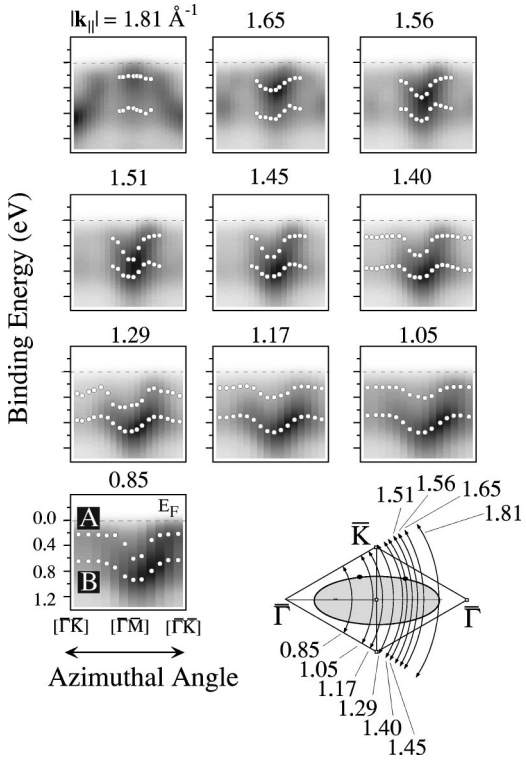


FIG. 7. Azimuthal ARPES sections through the second and the first SBZ of $1T$-$TaS_2$ for different parallel momenta, taken with 21.2 eV photons at 295 K. The radius is given on top of each section panel, respectively. The dashed line denotes the Fermi level. Bottom left: Energy and momentum scale valid for all panels. Peaks *A* and *B* (see text) are labeled. Bottom right: Sketch of the location where spectra have been taken with the parallel momenta indicated.

#### *2. Other directions in reciprocal space*

So far, we have concentrated solely on one high-symmetry direction. The question arises, what happens away from high-symmetry directions. In Fig. 7 we show azimuthal dispersion plots for a variety of parallel momenta. Spectra have been taken at RT with 21.2 eV and are displayed in linear gray scale plots with high intensity corresponding to black. Each azimuthal scan has been carried out along the circular trajectories given in the sketch [Fig. 7 (bottom right)]. The parallel momentum on top of each dispersion plot in Fig. 7 corresponds to the radius of the azimuthal scan. Spectra start in the $[\overline{\Gamma K}]$ direction and cover a range of 60°, i.e., they describe azimuthal cuts through the SBZ including the $[\overline{\Gamma M}]$ azimuth and, in particular, the two theoretically predicted Fermi-level crossings of the one-particle Ta $5d$ band in the $[\overline{KMK}]$ direction.[7,8] The labeling of the axes in the bottom left panel is valid for all plots.

For $|\mathbf{k}_\parallel| = 1.81$ Å$^{-1}$ and $|\mathbf{k}_\parallel| = 1.65$ Å$^{-1}$ in the dispersion plots (see Fig. 7), one observes at the boundaries (towards the $[\overline{\Gamma K}]$ azimuths) the elliptic features of the neighboring SBZ's. Therefore, we focus hereafter on the black feature evolving around the $[\overline{\Gamma M}]$ azimuth corresponding to the center of the dispersion plots. In all panels two peaks *A* and *B* are clearly identifiable. Their binding energies correspond reasonably well with the energies for two of the three CDW satellites calculated by Smith *et al.*[12] As emphasized above, we cannot exclude that the third CDW peak lies very close to $E_F$ and is not resolved due to the broad peaks. The evolution of the two clearly observable peaks *A* and *B* is, however, somewhat puzzling. In the 1.81-panel peak *A* can already be seen, but rather weak. On going to smaller momenta both peaks slightly shift to higher binding energies and the dispersion becomes stronger. That is what one expects when moving along the large half-axis of an ellipsoid towards the center (Fig. 7, bottom right). The effective binding-energy value increases till the maximum of 0.95 eV is reached in the center of the ellipse at $\mathbf{k}_\parallel = 1.05$ Å$^{-1}$. The important point is that we do *not* observe a clear distinct crossing of $E_F$ anywhere, analogous to what was demonstrated in the previous chapter. On approaching the center of the ellipse, the QP dispersion becomes larger and larger. *Both* peaks show dispersion and the energy difference stays approximately constant. This behavior is kept on further decreasing $|\mathbf{k}_\parallel|$. Most importantly, there is a characteristic change between the 1.56 panel and the 1.40 panel.

One observes for $|\mathbf{k}_\parallel| = 1.56$ Å$^{-1}$ that the intensity of peak *A* is larger than that of peak *B* at least around the $[\overline{\Gamma M}]$ azimuth. At $|\mathbf{k}_\parallel| = 1.51$ Å$^{-1}$ the intensity flips over to peak *B*, and it is this peak which then disperses and keeps the large spectral weight in the $|\mathbf{k}_\parallel| = 1.45$ Å$^{-1}$ and $|\mathbf{k}_\parallel| = 1.40$ Å$^{-1}$ spectra. Notice that peak *A* is always at least 300 meV away from $E_F$. The locations where both peaks undergo a backdispersing correspond to the locations where one would expect the Fermi vectors according to the theoretical one-particle ellipse. As a summary, the dispersion of two QP bands is observed, yet with a small bandwidth. Considerable dispersion takes place only when the band is *inside* the one-particle ellipse; *outside* the ellipse the bands are quasilocalized, as expected from the correlated low-temperature states in the *C* phase.

In summary, there are no Fermi-energy crossings detectable in the QC phase of $1T$-$TaS_2$. We believe that an onset of the Mott localization is responsible for this, meaning that the Fermi level lies in a pseudogap created by tails of the two overlapping Hubbard subbands. For the QC-*C* phase transition, this is an experimentally well-known fact,[14–16] but for ambient temperature, this is new. Hubbard bands, then, are a direct proof of electron-electron interaction. In addition, the presence of CDW's directly proves electron-phonon interactions. Consequently, the QC phase of $1T$-$TaS_2$ yields a strong interplay between electron-electron and electron-phonon interactions.

Finally, we have to consider recent theoretical work where it was shown that a pseudogap may arise intrinsically in photoemission from Ohmic losses in poorly conducting solids.[54] For the example of $La_{0.67}Ca_{0.33}MnO_3$, it is shown that the pseudogap at room temperature can be reconstructed invoking Ohmic losses at the surface. In the case of $1T$-$TaS_2$, the pseudogap becomes deeper upon decreasing the temperature and increasing the resistivity, however, because the QP features become sharper and *not* because of increased energy losses or broadening.[15,16] This is in contrast to what is anticipated from intrinsic losses where one expects a broadening of spectral features near $E_F$. As a consequence, in our case the pseudogap is indeed of different origin than the one predicted by Joynt.[54]

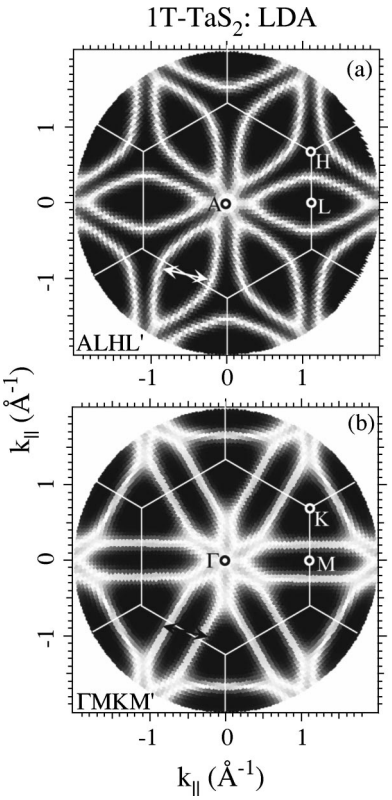


FIG. 8. FLAPW band-structure calculation of the Fermi surface of $1T$-$TaS_2$ using the WIEN97 code (Ref. 46). Shown are the results for two different Fermi-surface planes, namely the $ALHL'$ plane ($k_\perp = \pm \pi/a$) in (a) and the $\Gamma MKM'$ plane ($k_\perp = 0$ Å$^{-1}$) in (b).

### B. Localization vs Fermi-surface nesting

So far we have seen fingerprints for electron-electron and electron-phonon interactions. In 2D systems FS nesting has been assigned to be a possible driving force for the formation of CDW's. Now we address the question of FS nesting with respect to the topology of the FS in $1T$-$TaS_2$.

We performed band-structure calculations to calculate the FS of the undistorted state for two different planes. The results are shown in Fig. 8. Figure 8(a) shows the calculated FS in the $ALHL'$ plane. The corresponding undistorted BZ is superposed (white hexagons). White corresponds to points on the FS. Figure 8(b) gives the calculation for the $\Gamma MKM'$ plane, i.e., for a perpendicular momentum $\mathbf{k}_\perp = \pi/a$ shifted with respect to the $ALHL'$ plane (see Fig. 1). One can see that in the $\Gamma MKM'$ plane parallel FS sheets do exist perpendicular to the $MK$ line, whereas in the $ALHL'$ plane the elliptic FS pocket tapers off more distinctly towards the $A$ points. Taking into account that the FS measurement (e.g., with 21.2 eV) approximately follows a spherical final state, we can directly attribute the peaked structures from the FS measurement (cf. Fig. 9) to $\mathbf{k}_\perp$ effects. This has already been pointed out by Myron *et al.*,[8] but an experimental proof was lacking. In other words, effects of the perpendicular momentum do play a role and they may as well account for possible nesting vectors with components along $\mathbf{k}_\parallel$ and $\mathbf{k}_\perp$. For comparison, we also plotted vectors in Fig. 8, shown as arrows in the respective lower left parts. These ''nesting'' vectors display what is expected from the $(\sqrt{13}\times\sqrt{13})$ superstructure, i.e., a vector with magnitude equal to $1/\sqrt{13}\,|\overline{\Gamma\Gamma}|$ and rotated by 13.9° with respect to the $MK$ line. Nesting does not appear to be very likely in the $ALHL'$ plane [Fig. 8(a)]. In the $\Gamma MKM'$ plane it seems to be better, but not at all perfect. From theory, consequently, we have to consider that nesting might occur between different points of $\mathbf{k}_\perp$. Nonetheless, nesting does not seem to be perfect, and possible effects with respect to $\mathbf{k}_\perp$ have to be considered.

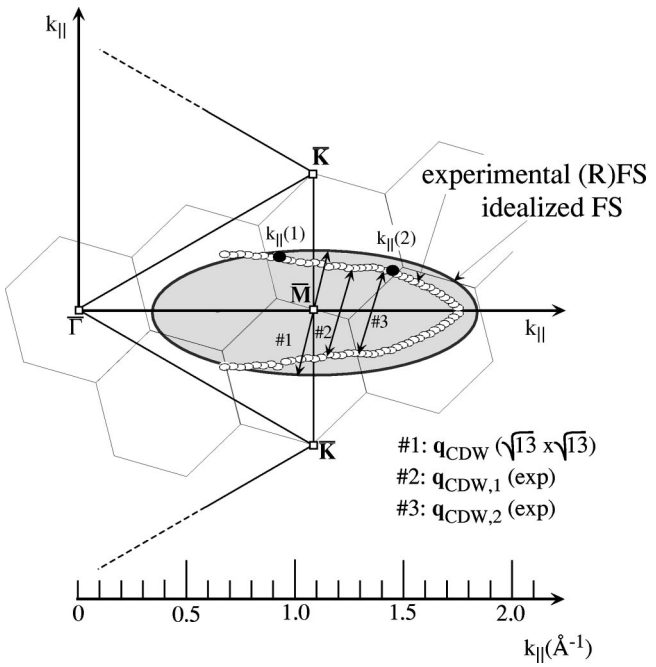


FIG. 9. True to scale sketch of the ''FS'' of $1T$-$TaS_2$ in the QC phase at room temperature. The triangle $\triangle(\overline{\Gamma KMK})$ yields the $(1\times1)$ SBZ, the small hexagons the reconstructed SBZ. The gray ellipse shows an idealized one-particle FS. The white ellipses on the FS show the locations of our ''Fermi vectors.'' The scale of the $\mathbf{k}_\parallel$ axes is given at the bottom. The nesting vectors and the points $\mathrm{k}_\parallel(1,2)$ are explained in the text.

For the sake of convenience, we give in Fig. 9 a sketch of an idealized one-particle Ta $5d$ FS shown as the gray-shaded ellipse around the $\overline{M}$ point. The irreducible wedge of the $(1\times1)$ SBZ is given by the thick triangle $\triangle(\overline{\Gamma KMK})$. In addition, we superposed the SBZ according to the $\sqrt{13}\times\sqrt{13}$ superstructure (small hexagons). At the bottom the scale is given for the $k_\parallel$ axis. To find the true RFS locations, we performed FSM at RT with He I$\alpha$ with a very high point density.[35] We received a set of angle pairs $(\theta,\phi)$ and the corresponding locations in $\mathbf{k}$ space are indicated by small white ellipses. The part below the $\overline{\Gamma M}$ axis has been obtained by reflecting the data above with respect to this axis, being consistent with the $D_{3d}^3$ space group. Points on the RFS formation inside than 0.7 Å$^{-1}$ are difficult to obtain because in these regions the structures in the azimuthal scans become broad[35] due to contributions from adjacent ellipses from neighboring irreducible wedges. The arrows 1–3 show possible nesting vectors $\mathbf{q}_{\mathrm{cdw}}$. Vector 1 corresponds to the $(\sqrt{13}\times\sqrt{13})$ superstructure, whereas vectors 2 and 3 are *arbitrarily* chosen from approximately parallel sections of the experimental RFS. The two black circles at $\mathbf{k}_\parallel(1)$ and $\mathbf{k}_\parallel(2)$ on the RFS show the onsets of reduced intensity near $E_F$ (see Fig. 10). They have been obtained by plotting the intensity of

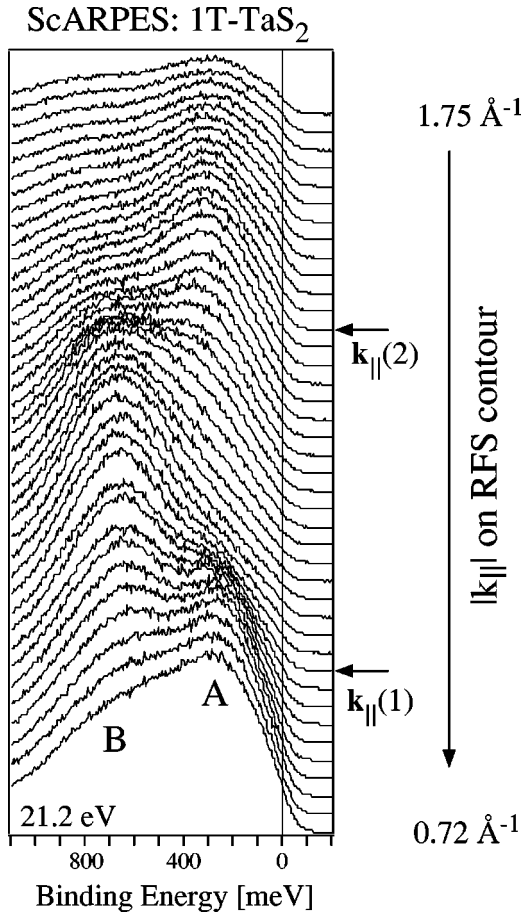


FIG. 10. Scanned ARPES spectra of $1T$-$TaS_2$ at room temperature with 21.2 eV *on* the ''RFS'' contour (Ref. 23). The meaning of the peaks *A* and *B* is given in the text. The arrows $\mathbf{k}_{\|}(1,2)$ show the onsets where peak *A* loses spectral weight (see text).

peak *A* (see Fig. 10) as a function of the parallel momentum (not shown here) and denote those points in **k** space where peak A starts losing spectral weight. The spectra in Fig. 10 were measured at RT with He I$\alpha$ radiation along the RFS contour (Fig. 9). The ScARPES spectra show a two-peak structure with binding energies of 300 meV (peak *A*) and 800 meV (peak *B*) corresponding to two CDW, induced satellites. The third peak, expected to be induced from the CDW potential cannot be seen clearly. As it develops into the LHB with decreasing *T*, we cannot exclude that it is lying close to $E_F$ hidden by the broad, incoherent background. Moreover, the ScARPES spectra are in perfect agreement with the data shown above away from high-symmetry directions.

The chosen nesting vectors (2 and 3) are arbitrary in length but have the correct direction, i.e., they are rotated by $\approx 13°$ away from the $[\overline{KMK}]$ line according to the $(\sqrt{13} \times \sqrt{13})$ superstructure. In addition, vectors connecting FS sheets become larger on approaching the $\overline{M}$ point. The deviation from the exact value for the *C* phase, i.e., $1/\sqrt{13}|\Gamma\Gamma| = 0.277|\Gamma\Gamma|$, is then decreasing. For example, the vector 3 has a value of $\approx 0.21|\Gamma\Gamma|$. This indicates that nesting may be *imperfect*.[55] The fact that the vectors become smaller farther away from $[\overline{KMK}]$ can be explained by $\mathbf{k}_{\perp}$ effects as argued before.

In a picture where nesting plays a role one expects a loss of spectral weight directly *around* $E_F$. In a mean-field (MF) approach the gap size $\Delta$ is given by $2\Delta = 3.52 k_B T_{CDW}^{MF}$,[33] $k_B$ being the Boltzmann's constant and $T_{CDW}^{MF}$ representing the respective transition temperature. This yields gaps of 53 meV for a transition temperature of 350 K (IC-QC transition) and 83 meV for 550 K (''no CDW''-IC transition), respectively. However, we see the intensity loss for peak *A* $\approx 300$ meV away from the chemical potential. We believe that this decrease of spectral weight comes from the fact that one enters the region where the quasilocalized satellite peaks start to follow the original dispersing one-particle-like Ta $5d$ band (cf. Fig. 7). The spectra at $\mathbf{k}_{\|}(1)$ and $\mathbf{k}_{\|}(2)$ coincide with those spectra of the azimuthal dispersion plots where the intensity of peaks *A* and *B* in Fig. 7 flips. In other words, the spectra on the RFS (Fig. 10) do more likely show effects of the experimental band structure, which is totally determined by the interplay between the CDW-induced satellites and the remaining one-particle band which becomes less and less distinct with decreasing temperature.

As a final point we emphasize that we do not observe any backfolding of bands at all on the contour of the RFS due to the $\sqrt{13} \times \sqrt{13}$ superstructure (see Fig. 9). Backfolding effects have not been seen as well in the electronic band structure below $E_F$ being consistent with all previous ARPES work. This nonobservation cannot be generalized for all $1T$ polytypes since $1T$-$TiSe_2$ exhibits a $(2\times2\times2)$ reconstruction and, in that case, the Se bands near normal emission exhibit a backfolding due to the new symmetry.[31,56,57] The lack of signs in the data related to backfolding effects may be explained by the small size of reconstructed BZ's (see Fig. 2) or as well by small Fourier components of the CDW potential as argued earlier.[48]

## V. SUMMARY AND OUTLOOK

We examined in detail the electronic band structure of the RT phase of $1T$-$TaS_2$ by means of scanned ARPES. In particular, we demonstrated that no crossings of the Fermi level are visible, indicating that a correlation pseudogap due to electron-electron interaction of electrons in the Ta $5d$ derived band exists already at RT. The magnitude of the gap is difficult to determine because of the inherent broadening of the spectral function at RT.

Moreover, we found that the complete RT band structure is governed by two quasiparticle peaks, which can be assigned to stem from the outerlying shells of the ''Star-of-David'' cluster related to the formation of CDW's in this material. Those peaks show a quasilocalized dispersion behavior outside the one-particle ellipsoid and follow the free-electron-like dispersion inside the ellipsoid. We do not find QP weight which can be attributed to a coherent LHB state; rather, we find a pseudogap present at RT and a broad background possibly due to fluctuations of this inherent ''quasiparticle liquid'' that constitutes the remnant Fermi surface. All spectral features seem to account for the pseudogap in that they show a backdispersing at the normal state Fermi vectors.

Upon addressing the particular question of possible FS nesting, we scanned the remnant FS and found a considerable decrease of spectral weight around the high-symmetry

line [$\overline{KMK}$]. However, this distinct decrease is obtained for a peak situated 300 meV below $E_F$. Nesting appears to be rather imperfect, because of a lack of extended parallel and gapped portions on the FS. To further explore the mechanisms at work in 1*T*-$TaS_2$, ScARPES spectra need to be collected in a narrow temperature window around the CDW transitions at 350 and 550 K. Broadening due to the elevated temperatures might, however, hamper, if not render impossible, these attempts.

**ACKNOWLEDGMENTS**

We benefited from fruitful discussions with M. Grioni, R. Claessen, Th. Straub, R. Noack, D. Baeriswyl, and K. Maki. The outstanding help of our mechanics and electronics workshop with O. Raetzo, E. Mooser, R. Schmid, O. Zosso, Ch. Neururer, and F. Bourqui is gratefully acknowledged. This work has been supported by the Fonds National Suisse pour la Recherche Scientifique.

*Present Address: Institut de Physique, Université de Neuchâtel, Rue A.-L. Breguet 1, CH-2000 Neuchâtel, Switzerland. E-mail address: thorsten.pillo@iph.unine.ch

[1] J.A. Wilson and A.D. Yoffe, Adv. Phys. **18**, 193 (1969).
[2] J.A. Wilson, F.J. Di Salvo, and S. Mahajan, Adv. Phys. **24**, 117 (1975).
[3] M. Grioni and J. Voit, in *Electron Spectroscopies Applied to Low-Dimensional Materials*, edited by H. Stanberg and H. Hughes (Kluwer, Dordecht, 1999), and references therein.
[4] R.V. Coleman, B. Giambattista, P.K. Hansma, A. Johnson, W.W. McNairy, and C.G. Slough, Adv. Phys. **37**, 559 (1988).
[5] F.J. Di Salvo, J.A. Wilson, B.G. Bagley, and J.V. Waszczak, Phys. Rev. B **12**, 2220 (1975).
[6] P. Fazekas and E. Tosatti, Philos. Mag. B **39**, 229 (1979); Physica B & C **99**, 183 (1980).
[7] A.M. Woolley and G. Wexler, J. Phys. C **10**, 2601 (1977).
[8] H.W. Myron and A.J. Freeman, Phys. Rev. B **11**, 2735 (1975).
[9] R. Mamy, P. Thiry, G. Vachier, and A. Couget, J. Phys. (France) Lett. **42**, L79 (1981).
[10] N.V. Smith and M.M. Traum, Phys. Rev. B **11**, 2078 (1975).
[11] R.A. Pollak, D.E. Eastman, F.J. Himpsel, P. Heimann, and B. Reihl, Phys. Rev. B **24**, 7435 (1981).
[12] N.V. Smith, S.D. Kevan, and F.J. Di Salvo, J. Phys. C **18**, 3175 (1985).
[13] R. Manzke, O. Anderson, and M. Skibowski, J. Phys. C **21**, 2399 (1988).
[14] R. Manzke, T. Buslaps, B. Pfalzgraf, M. Skibowski, and O. Anderson, Europhys. Lett. **8**, 195 (1989).
[15] B. Dardel, M. Grioni, D. Malterre, P. Weibel, Y. Baer, and F. Lévy, Phys. Rev. B **45**, 1462 (1992).
[16] B. Dardel, M. Grioni, D. Malterre, P. Weibel, Y. Baer, and F. Lévy, Phys. Rev. B **46**, 7407 (1992).
[17] F. Zwick, H. Berger, I. Vobornik, G. Margaritondo, L. Forró, M. Onellion, G. Panaccione, A. Taleb, and M. Grioni, Phys. Rev. Lett. **81**, 1058 (1998).
[18] X. Wu and C. Lieber, Science **243**, 1703 (1989); Phys. Rev. Lett. **64**, 1150 (1990).
[19] B. Giambattista, C.G. Slough, W.W. McNairy, and R.V. Coleman, Phys. Rev. B **41**, 10 082 (1990).
[20] W. Han, R.A. Pappas, E.R. Hunt, and R.F. Frindt, Phys. Rev. B **48**, 8466 (1993).
[21] B. Burk, R.E. Thomson, A. Zettl, and J. Clarke, Phys. Rev. Lett. **66**, 3040 (1991).
[22] J.J. Kim, W. Yamaguchi, T. Hasegawa, and K. Kitazawa, Phys. Rev. Lett. **73**, 2103 (1994).
[23] Th. Pillo, J. Hayoz, H. Berger, M. Grioni, L. Schlapbach, and P. Aebi, Phys. Rev. Lett. **83**, 3494 (1999).
[24] Th. Straub, Ph.D. thesis, University of Saarbrücken Germany, 1998.
[25] Th. Pillo (unpublished).
[26] J.A. Wilson, F.J. Di Salvo, and S. Mahajan, Phys. Rev. Lett. **32**, 882 (1974).
[27] F.J. Di Salvo and J.E. Graebner, Solid State Commun. **23**, 825 (1977).
[28] A.H. Thompson, F.R. Gamble, and J.F. Revelli, Solid State Commun. **9**, 981 (1971).
[29] C.B. Scruby, P.M. Williams, and G.S. Parry, Philos. Mag. **31**, 255 (1975).
[30] R. Brouwer and F. Jellinek, Physica B & C **99B**, 51 (1980).
[31] O. Anderson, R. Manzke, and M. Skibowski, Phys. Rev. Lett. **55**, 2188 (1985).
[32] W. Geertsma, C. Haas, R. Huisman, and F. Jellinek, Solid State Commun. **10**, 75 (1972).
[33] G. Grüner, *Density Waves in Solids*, Frontiers in Physics, Vol. 89 (Addison-Wesley, Reading, MA, 1994).
[34] R. E. Peierls, *Quantum Theory of Solids* (Oxford University Press, New York, 1955).
[35] Th. Pillo, J. Hayoz, P. Aebi, and L. Schlapbach, J. Electron Spectrosc. Relat. Phenom. **101-103**, 811 (1999).
[36] J. Osterwalder, T. Greber, S. Hüfner, and L. Schlapbach, Phys. Rev. B **44**, 13 764 (1991).
[37] E. Boschung, Th. Pillo, J. Hayoz, L. Patthey, P. Aebi, and L. Schlapbach, Phys. Rev. B **58**, R10 102 (1998).
[38] Th. Pillo, L. Patthey, E. Boschung, J. Hayoz, P. Aebi, and L. Schlapbach, J. Electron Spectrosc. Relat. Phenom. **57**, 243 (1998).
[39] H. Berger (unpublished).
[40] P. Aebi, J. Osterwalder, P. Schwaller, L. Schlapbach, M. Shimoda, T. Mochiku, and K. Kadowaki, Phys. Rev. Lett. **72**, 2757 (1994).
[41] P. Aebi, T.J. Kreutz, J. Osterwalder, R. Fasel, P. Schwaller, and L. Schlapbach, Phys. Rev. Lett. **76**, 1150 (1996).
[42] Th. Straub, R. Claessen, P. Steiner, S. Hüfner, V. Eyert, K. Friemelt, and E. Bucher, Phys. Rev. B **55**, 13 473 (1998).
[43] J. Osterwalder, Surf. Rev. Lett. **4**, 391 (1997) and references therein.
[44] T.J. Kreutz, T. Greber, P. Aebi, and J. Osterwalder, Phys. Rev. B **58**, 1300 (1998).
[45] Th. Pillo, J. Hayoz, P. Aebi, and L. Schlapbach, Physica B **259-261**, 1118 (1999).
[46] P. Blaha, K. Schwarz, and J. Juitz, WIEN97, Vienna University of Technology (improved and updated UNIX version of the original copyrighted WIEN code), published by P. Blaha, K. Schwarz, P. Sorantin, and S.B. Trickey, Comput. Phys. Commun. **59**, 399 (1990).
[47] J.P. Perdew, S. Burke, and M. Ernznerhof, Phys. Rev. Lett. **77**, 3865 (1996).
[48] R. Claessen, B. Burandt, H. Carstensen, and M. Skibowski, Phys. Rev. B **41**, 8270 (1990).
[49] The room-temperature measurements in the $\Gamma ALM$ plane have

been performed with unmonochromatized He I radiation. A careful subtraction of He I$\beta$ satellite radiation-induced peaks has been carried out.

[50] V. Eyert (private communication).

[51] R. Liu, C.G. Olson, W.C. Tonjes, and R.F. Frindt, Phys. Rev. Lett. **80**, 5762 (1998).

[52] B. Dardel, M. Grioni, D. Malterre, P. Weibel, Y. Baer, and F. Lévy, J. Phys.: Condens. Matter **5**, 6111 (1993).

[53] R. Claessen, R.O. Anderson, J.W. Allen, C.G. Olson, C. Janowitz, W.P. Ellis, S. Harm, M. Kalnig, R. Manzke, and M. Skibowski, Phys. Rev. Lett. **69**, 808 (1992).

[54] R. Joynt, Science **284**, 777 (1999); A.J. Arko, *ibid.* **284**, 752 (1999).

[55] G.H. Gweon, J.D. Denlinger, J.A. Clack, J.W. Allen, C.G. Olson, E. DiMasi, M.C. Aronson, B. Foran, and S. Lee, Phys. Rev. Lett. **81**, 886 (1998).

[56] N.G. Stoffel, S.D. Kevan, and N.V. Smith, Phys. Rev. B **31**, 8049 (1985).

[57] Th. Pillo, J. Hayoz, H. Berger, F. Lévy, L. Schlapbach, and P. Aebi, Phys. Rev. B **61**, 16 213 (2000).